PTEP

Prog. Theor. Exp. Phys. **2018**, 013A02 (15 pages)
DOI: 10.1093/ptep/ptx172

Remarkable similarities of two pairs of stable and saddle canards in a van der Pol oscillator under extremely weak periodic perturbation

Yuta Nagata[1], Naohiko Inaba[2,*], Munehisa Sekikawa[3], Tetsuro Endo[1], Ken'ichi Fujimoto[4], and Tetsuya Yoshinaga[5]

[1]*Department of Electronics and Bioinformatics, Meiji University, Kawasaki 214-8571, Japan*
[2]*Organization for the Strategic Coordination of Research and Intellectual Properties, Meiji University, Kawasaki 214-8571, Japan*
[3]*Department of Mechanical and Intelligent Engineering, Utsunomiya University, Utsunomiya 321-8585, Japan*
[4]*University Consortium for e-Learning, Shikoku Center, Kagawa University, Takamatsu 760-8521, Japan*
[5]*Institute of Biomedical Sciences, Tokushima University, Tokushima 770-8509, Japan*
*E-mail: naohiko@yomogi.jp

Received October 28, 2017; Accepted November 11, 2017; Published January 9, 2018

Canards are interesting nonlinear phenomena that have generated intense research interest since their discovery in the late 20th century. We are interested here in how canard-generating dynamics are influenced by extremely weak periodic perturbations that cause the formation of saddle-node bifurcations in the fundamental harmonic entrainment region. In a previous study, we discovered that another entrainment region exists within the fundamental harmonic entrainment region surrounded by the second saddle-node bifurcation curves. We found that two pairs of stable and saddle canards coexist in this second entrainment region under such weak periodic perturbation. Moreover, the stable and saddle canards are matched pairwise; i.e., each stable canard quite closely resembles a corresponding saddle canard. Calculation of the correlation coefficients of the four canards revealed two similar solutions on the order of $0.9999\cdots$ between the two pairs of similar canards. In contrast, the correlation coefficients of the dissimilar canards differ from unity in proportion to the difference between the given bifurcation parameter value and the parameter values at the saddle-node bifurcation points. Approximately, they take values from 0.998 to 0.975. These contrasts are noteworthy. Similar bifurcation phenomena were observed in the $1/2$-subharmonic entrainment region. We hypothesize that the two pairs of stable and saddle canards are invariant with respect to a slight shift of time at the saddle-node bifurcation points, and we numerically prove that such a property approximately holds at the bifurcation points.

Subject Index A55, A56

1. Introduction

Canard phenomena are one of the major discoveries in the field of nonlinear dynamics in the late 20th century and have been extensively studied during the past three decades [1–10]. Canards can be generated in simple singularly perturbed second-order autonomous differential equations that include a small parameter ε. Let us consider the van der Pol equation in the following form:

$$\begin{aligned} \varepsilon\dot{x} &= y + x(1 - x^2), \\ \dot{y} &= -x + B_0, \end{aligned} \tag{1}$$

where ε is assumed to be small. An intersection of the x-nullcline $y = -x(1-x^2)$ and the y-nullcline $x = B_0$ is an equilibrium; if $|B_0| < 1/\sqrt{3}$, it is unstable, and if $|B_0| > 1/\sqrt{3}$, it becomes stable. A supercritical Andronov–Hopf bifurcation (AHB) occurs at $B_0 = \pm 1/\sqrt{3}$. A remarkable phenomenon is observed when B_0 is chosen to be slightly under $1/\sqrt{3}$ (or slightly over $-1/\sqrt{3}$). The amplitude of the oscillation is extremely sensitive to B_0. Nonstandard analysis [5] has shown that the amplitude of the oscillation is changed on the order of 1 if $|B_0|$ decreases on the order of $\exp(-1/\varepsilon)$. At $\varepsilon = 0.1$ and 0.01, the magnitude of $\exp(-1/\varepsilon)$ approximates 5×10^{-5} and 4×10^{-44}, respectively. As the shape of the oscillation in the phase plane resembles a duck (French canard), it was named a "canard" [5].

We now ask how canards in dynamical systems are influenced by extremely weak periodic perturbations of amplitude on the order of $\exp(-1/\varepsilon)$. Sekikawa et al. proposed the following nonautonomous dynamics derived from a forced van der Pol oscillator [10]:

$$\begin{aligned} \varepsilon \dot{x} &= y + x(1 - x^2) \\ \dot{y} &= -x + B_0 + B \sin \omega\tau . \end{aligned} \tag{2}$$

They discovered that a second entrainment region surrounded by saddle-node bifurcations and containing two coexisting canards is generated inside the fundamental harmonic entrainment region. Here, a canard is defined as a closed orbit following both attracting and repelling slow manifolds. Such bifurcation structures are observed in several subharmonic and fractional harmonic entrainment regions in the van der Pol equation under such weak periodic perturbation [10].

In this study, we investigate the characteristics of these coexisting canards. The saddle-node bifurcations generate a saddle solution as well as a stable solution. According to our numerical results, we find that the saddle solutions generated by each saddle-node bifurcation are also canard-shaped in the phase plane. The first pair of stable and saddle canards is born from a saddle-node bifurcation that forms the fundamental harmonic entrainment region, while the second pair originates from the second saddle-node bifurcation inside the fundamental harmonic entrainment region. Such nested entrainment regions caused by sequential saddle-node bifurcations represent a newly discovered bifurcation structure in nonautonomous oscillators that we have identified for the first time. In this structure, noteworthy phenomena are observed slightly after the generation of the second saddle-node bifurcation. We found that the stable canard arising from the first saddle-node bifurcation resembles the saddle canard from the second saddle-node bifurcation quite closely, although they differ significantly in phase. Similarly, the saddle canard born of the first saddle-node bifurcation closely resembles the stable canard arising from the second saddle-node bifurcation.

We calculate the correlation coefficients of each $y(\tau + \theta_0)$, where θ_0 is chosen such that $y(\theta_0) = 0$ and $\dot{y}(\theta_0) > 0$. When B is chosen on the order of $\exp(-1/\varepsilon)$, the correlation coefficient of the stable canard of the first saddle-node bifurcation and the saddle canard of the second saddle-node bifurcation is $0.9999\cdots$ if the bifurcation parameter is not close to the saddle-node bifurcation points that generate the dissimilar stable and saddle canards. Similarly, the correlation coefficients between the stable canard arising from the second saddle-node bifurcation and the saddle canard from the first saddle-node bifurcation are consistently $0.9999\cdots$. Because they resemble each other quite well, it is practically impossible to differentiate these stable and saddle canards arising from closed orbits projected onto the phase plane. In contrast, according to our numerical results, the correlation coefficients of the dissimilar canards decrease monotonically from unity in proportion to the difference between the given bifurcation parameter value and the parameter values of the saddle-node bifurcation points. We hypothesized that similar stable and saddle canards are generated as a result of a saddle-node bifurcation for which the Jacobian matrix has an eigenvector of 1.0 and

attempted to verify this conjecture. Although the hypothesis approximately holds according to our numerical results, we still could not distinguish the saddle-node bifurcations that generate similar stable or dissimilar stable and saddle canards.

We also verified that a similar bifurcation structure can be observed in the 1/2-subharmonic entrainment region.

2. Van der Pol oscillator under weak periodic perturbation and canards

Figure 1 shows a circuit diagram of a forced van der Pol oscillator. In the figure, C and L denote capacitance and inductance, respectively, E_1 is a DC power supply, and $E_2 \sin(\omega' t)$ is an AC power supply. The term *N.C.* represents a nonlinear conductance. We assume that the $v - i$ characteristic of the nonlinear conductance $i_n(v)$ can be represented by the following third-order polynomial function:

$$i_n(v) = -g_1 v + g_3 v^3, \ \ g_1 > 0, g_3 > 0. \tag{3}$$

From Kirchhoff's law, the governing equation of the circuit is represented by the following second order nonautonomous ordinary differential equations:

$$\begin{aligned} C\frac{dv}{dt} &= i - i_n(v), \\ L\frac{di}{dt} &= -v + E_1 + E_2 \sin(\omega' t). \end{aligned} \tag{4}$$

We assume that C is small and E_2 is extremely small. Rescaling then produces

$$\begin{gathered} \varepsilon = \frac{C}{g_1^2 L}, \ B_0 = \sqrt{\frac{g_3}{g_1}} E_1, B = \sqrt{\frac{g_3}{g_1}} E_2, t = g_1 L \tau, \ \omega' = g_1 L \omega, \\ \frac{d}{d\tau} = \cdot, \ x = \sqrt{\frac{g_3}{g_1}} v, \ y = \sqrt{\frac{g_3}{g_1^3}} i, \end{gathered} \tag{5}$$

and the normalized equation represented by Eq. (2). Throughout the discussion, we set $\varepsilon = 0.1$ and B is on the order of $\exp(-1/\varepsilon)$.

Figure 2 shows stable solutions in the absence of perturbation ($B = 0$). The significant change of the amplitude under slight variation of B_0 is called a "canard explosion".

In our previous works [9,10], we discovered that two canard-shaped attractors coexist in some synchronization regions under such small periodic perturbations. These pairs are born as a consequence of two successive saddle-node bifurcations and, because saddle-node bifurcations generate

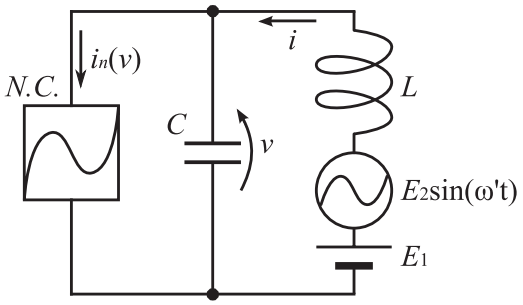

Fig. 1. Circuit diagram of a forced van der Pol oscillator.

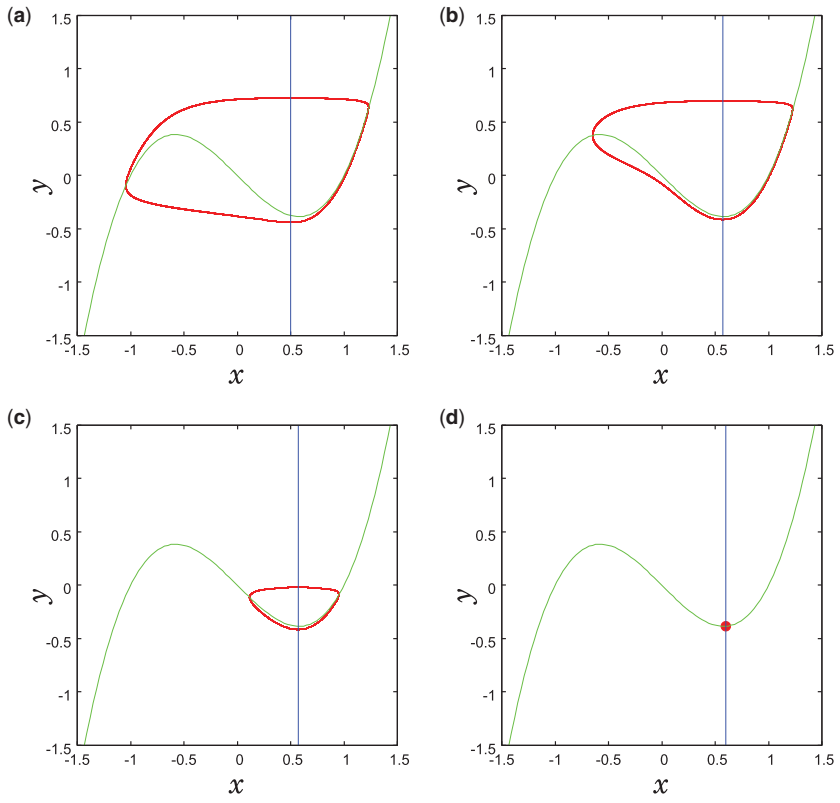

Fig. 2. Attractors of Eq. (2) for $\varepsilon = 0.1$ and $B = 0$. (a) Large periodic orbit ($B_0 = 0.5$), (b) canard ($B_0 = 0.569\,44$), (c) small periodic orbit ($B_0 = 0.5695$), (d) equilibrium point ($B_0 = 0.6$).

a pair of stable and saddle solutions, the saddle solutions must exist. In this section, B and ω are chosen inside the second saddle-node bifurcation curves [10] generated in the fundamental harmonic entrainment region. According to our numerical results, the two saddle solutions in this entrainment region are also canard-shaped in the phase plane. Hereafter, we call the stable and saddle canards arising from the first saddle-node bifurcation stable canard 1 and saddle canard 1, respectively. Similarly, we call the stable and saddle canard arising from the second saddle-node bifurcation stable canard 2 and saddle canard 2, respectively. The two stable solutions and two saddle solutions are illustrated in Fig. 3 as an example. Successive saddle-node bifurcations and their entrainment regions are discussed in detail in the next section. Figure 4 presents the waveforms of the four canards. We see that the waveform of stable canard 1 resembles that of saddle canard 2, although the phases of these two canards are significantly different. Similarly, the waveform of stable canard 2 resembles that of saddle canard 1. Actually, when we superpose Fig. 3(a) (resp. Fig. 3(c)) and Fig. 3(d) (resp. Fig. 3(b)), the two solutions almost overlap. Figure 5 shows a superposed view of the four canards presented in Figs. 3(a), (b), (c), and (d); we cannot distinguish the difference between stable canard 1 and saddle canard 2 (or between stable canard 2 and saddle canard 1) as long as we observe the solutions in the phase plane.

3. Analysis of the significant resemblance between the two pairs of stable and saddle canards in the fundamental harmonic entrainment region

To clarify the structural scenario in which each stable canard solution resembles each saddle canard solution, we draw a bifurcation diagram and show how the two pairs of canards are born. First, we

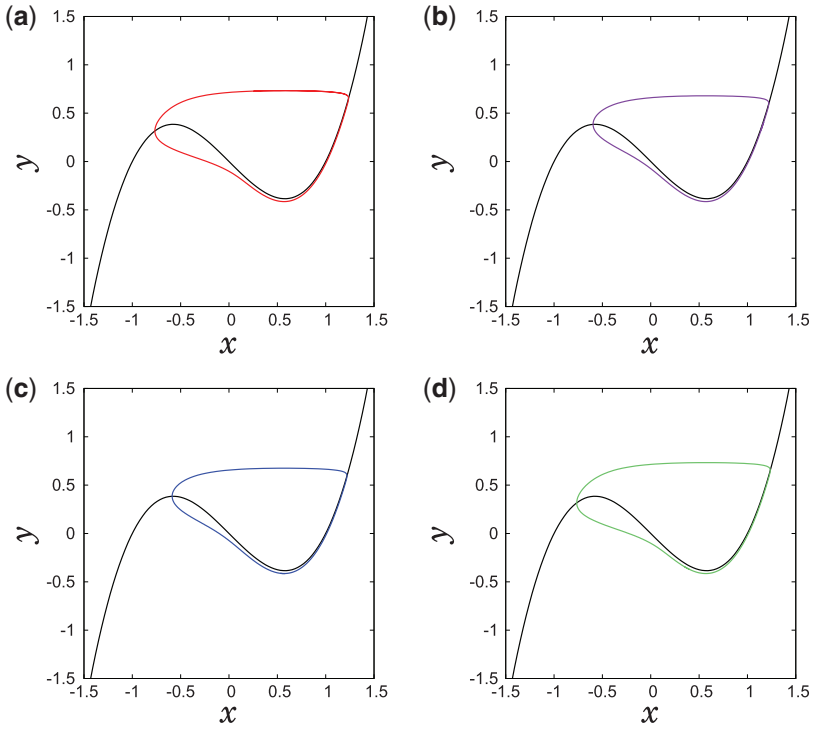

Fig. 3. Two coexisting pairs of stable and saddle canards obtained from Eq. (2) with $\varepsilon = 0.1$, $\omega = 1.19$, $B = 5.0 \times 10^{-5}$, and $B_0 = 0.569\,44$. This choice of parameters corresponds to A6 in Fig. 7. (a) Stable canard 1 with initial conditions $(x, y) = (0.204\,95, 0.726\,37)$ at $\tau = 0$. (b) Saddle canard 1 with initial conditions $(x, y) = (1.169\,81, 0.411\,77)$ at $\tau = 0$. (c) Stable canard 2 with initial conditions $(x, y) = (0.581\,27, -0.414\,28)$ at $\tau = 0$. (d) Saddle canard 2 with initial conditions $(x, y) = (0.403\,19, -0.372\,84)$ at $\tau = 0$.

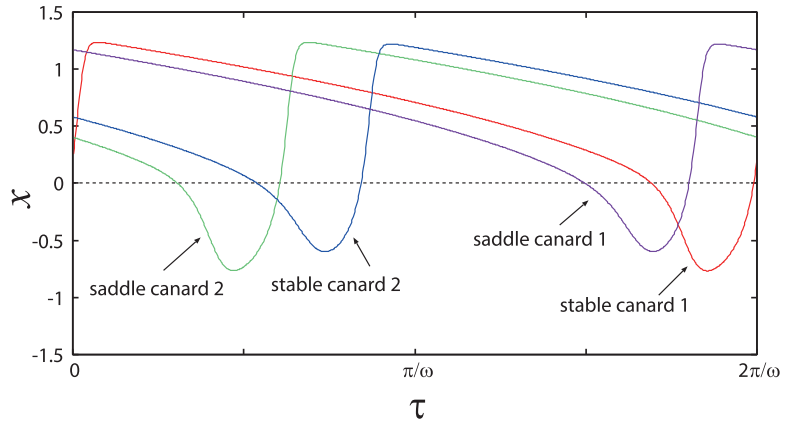

Fig. 4. Time series of the four canards in Fig. 3. Parameters are the same as those in Fig. 3.

define the stroboscopic Poincaré map as follows:

$$\begin{aligned} \mathrm{T}_\lambda \quad &: \quad \mathrm{R}^2 \to \mathrm{R}^2 \\ &\quad u_0 \mapsto \mathrm{T}_\lambda(u_0) \equiv \varphi(2\pi/\omega, u_0, \lambda), \end{aligned} \tag{6}$$

where $\varphi(\tau, u_0, \lambda)$ is the solution, $u_0 \equiv (x_0, y_0)^\top$ is an initial point at $\tau = 0$, and λ is a bifurcation parameter.

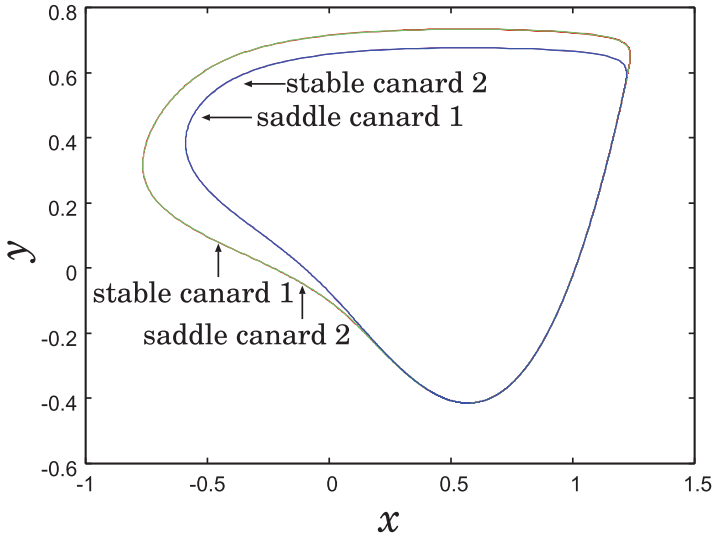

Fig. 5. Superposed illustration of the four canards from Fig. 3. The parameter values are the same as those in Fig. 3.

Let u_0 be an m-periodic point of T_λ. Then, u_0 satisfies

$$\mathrm{T}_\lambda^m(u_0) - u_0 = 0. \tag{7}$$

The characteristic equation is represented as follows:

$$\left| \frac{d}{du_0} \mathrm{T}_\lambda^m(u_0) - \mu I \right| = 0. \tag{8}$$

Let μ_1 and μ_2 ($|\mu_1| \geq |\mu_2|$) be the solutions of μ. If $0 < |\mu_2| < |\mu_1| < 1$, the m-periodic point is said to be a stable node. If $|\mu_1| > 1 > |\mu_2|$, the m-periodic point is said to be a saddle. If $|\mu_1| > |\mu_2| > 1$, the m-periodic point is said to be completely unstable. When $|\mu_1| = 1$, a bifurcation occurs. We analyze the case of $\mu_1 = 1$, in which a saddle-node bifurcation set is produced. To draw the bifurcation diagram, we adopt the shooting algorithm in Ref. [11]. Figure 6 shows a bifurcation diagram of the fundamental harmonic entrainment region surrounded by the two saddle-node bifurcation curves $\mathrm{G}_1(\mu_1 = 1)$. In this fundamental harmonic entrainment region, we find another entrainment region surrounded by another set of saddle-node bifurcation curves, which are denoted by G_2 [10]. To the best of our knowledge, the nested entrainment regions caused by the two saddle-node bifurcations G_1 and G_2 have not yet been observed in a forced oscillator. The four canards discussed in Figs. 3, 4, and 5 in the previous sections are obtained at point A6 in Fig. 6. A schematic diagram of this entrainment region is illustrated in the upper figure of Fig. 7. In the following discussion, we fix $B = 5 \times 10^{-5} \simeq \exp(-1/\varepsilon)|_{\varepsilon=0.1}$ on the line L_1 and vary ω on L_1 as a bifurcation parameter. The lower figure of Fig. 7 shows a schematic illustration of the fixed-point manifold. The saddle-node bifurcations occur at points Q_1, Q_2, Q_3, and Q_4 in Fig. 7. In the figure, ${}_i\mathrm{D}$ denotes a fixed point of unstable dimension; i.e., the solid curves denoted by ${}_0\mathrm{D}$ represent the stable fixed-point manifold and the dashed curves marked with ${}_1\mathrm{D}$ are the saddle fixed-point manifold. The numerically obtained fixed-point manifolds projected onto the ω–x and ω–y planes are shown in Figs. 8(a) and (b), respectively.

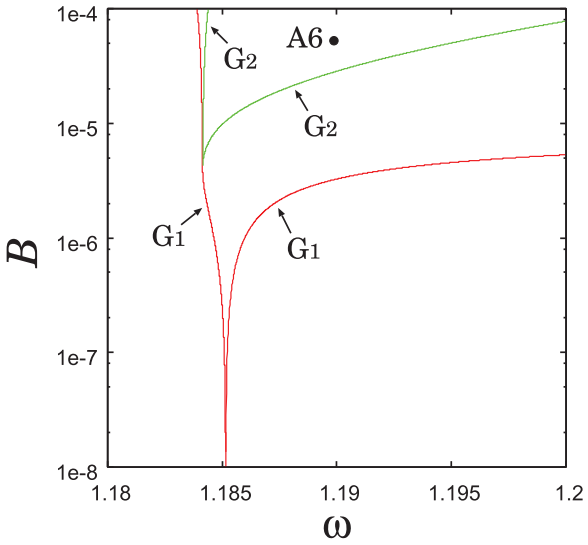

Fig. 6. Bifurcation diagram of the fundamental harmonic entrainment region for $\varepsilon = 0.1$ and $B_0 = 0.569\,44$. G_1 denotes the first saddle-node bifurcation set, while G_2 denotes the second saddle-node bifurcation set. The coordinates of A6 are given in Fig. 7.

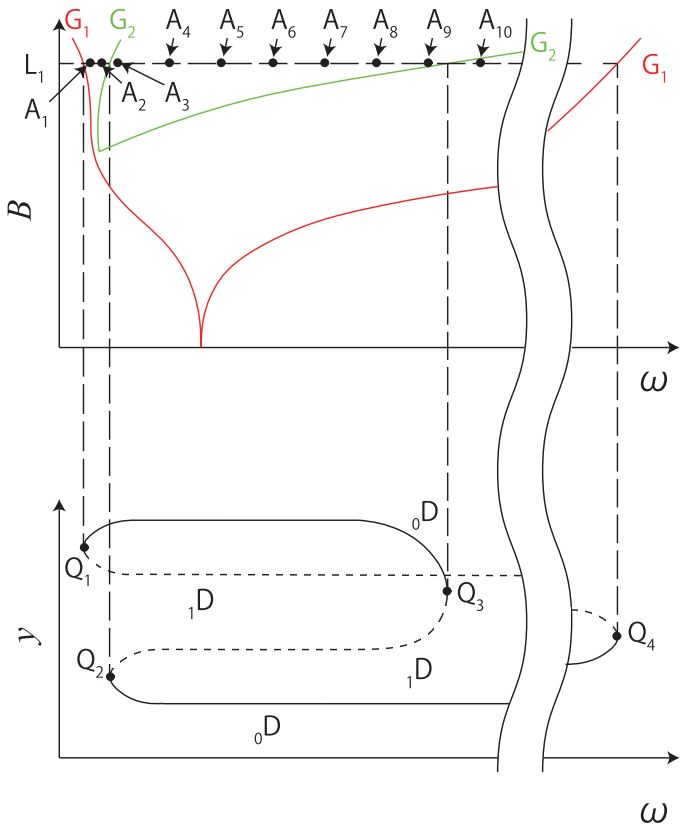

Fig. 7. Schematic bifurcation diagram of the fundamental harmonic entrainment region (upper) and the structure of the corresponding fixed-point manifold along L_1 (lower). The coordinates (ω,B) of the parameter points A_1–A_{10} are as follows: A_1: $(1.184\,03, 5 \times 10^{-5})$; A_2: $(1.184\,23, 5 \times 10^{-5})$; A_3: $(1.184\,27, 5 \times 10^{-5})$; A_4: $(1.1855, 5 \times 10^{-5})$; A_5: $(1.187, 5 \times 10^{-5})$; A_6: $(1.19, 5 \times 10^{-5})$; A_7: $(1.193, 5 \times 10^{-5})$; A_8: $(1.1945, 5 \times 10^{-5})$; A_9: $(1.194\,96, 5 \times 10^{-5})$; A_{10}: $(1.1955, 5 \times 10^{-5})$. Q_1–Q_4 are the saddle-node bifurcation points and Q_1 is at the immediate left of Q_2.

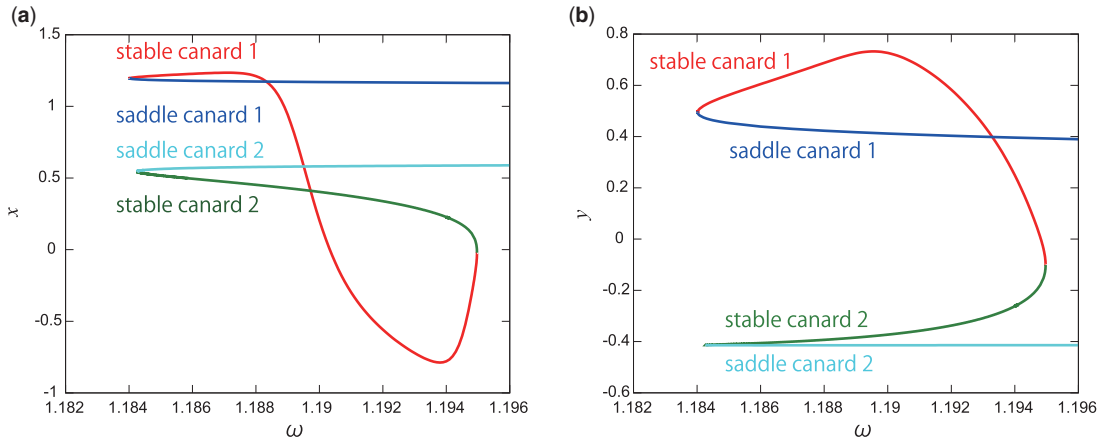

Fig. 8. Fixed-point manifold obtained numerically: (a) projected onto the ω–x plane and (b) projected onto the ω–y plane.

To investigate how the two pairs of stable and saddle canards resemble each other, we vary ω to observe the two pairs of stale and saddle canards projected onto the x–y phase plane.

We can analyze the nested bifurcation structures caused by the successive saddle-node bifurcations by tracing the bifurcation diagram of the fundamental harmonic entrainment region shown in Fig. 7 from left to right. Figures 9(c)–(i) show the four-canard solutions, while Figs. 9(a), (b), and (j) show the two-canard solutions. Figure 9(a) shows stable canard 1 and saddle canard 1 at A_1 immediately after the first saddle-node bifurcation point in Fig. 7. As A_1 is close to the curve G_1, these two canards nearly overlap in the phase plane. Because A_2 is significantly separated from G_1 in Fig. 9(b), we can detect the difference between stable canard 1 and saddle canard 1. Note that the fixed point of stable canard 1 on the Poincaré section (●) moves to some extent, while that of saddle canard 1 (○) moves little as ω is separated from G_1.

At the bifurcation point Q_2 in Fig. 7, the second saddle-node bifurcation occurs and another pair of stable canard 2 and saddle canard 2 is born, as illustrated in Fig. 9(c). The solid blue circle and the light green open circle denote the fixed points of stable canard 2 and the saddle canard 2 on the Poincaré section, respectively. In contrast to the former case, the light green open circle corresponding to saddle canard 2 begins to move significantly, while the blue solid circle corresponding to stable canard 2 moves only slightly as ω increases. This discrepancy is noteworthy.

Note that a qualitative change emerges slightly after the second saddle-node bifurcation. As shown in Figs. 9(d)–(i), following generation of the second saddle-node bifurcation at Q_2, a significant resemblance is observed between stable canard 1 and saddle canard 2 and between stable canard 2 and saddle canard 1. The fixed points of stable canard 1 (red) and saddle canard 2 (light green) are considerably separated, i.e., the phases of these two canard solutions are different, as shown in Fig. 4.

By increasing ω further, stable canard 1 and saddle canard 2 disappear through the saddle-node bifurcation at Q_3; similarly, stable canard 2 and saddle canard 1 disappear through the saddle-node bifurcation at Q_4.

To evaluate the similarities of the canard solutions, the correlation coefficients are defined as follows:

$$C(y,y') = \frac{\sum_{i=1}^{N}(y_i-\bar{y})(y'_i-\bar{y}')}{\sqrt{\sum_{i=1}^{N}(y_i-\bar{y})^2}\sqrt{\sum_{i=1}^{N}(y'_i-\bar{y}')^2}}, \tag{9}$$

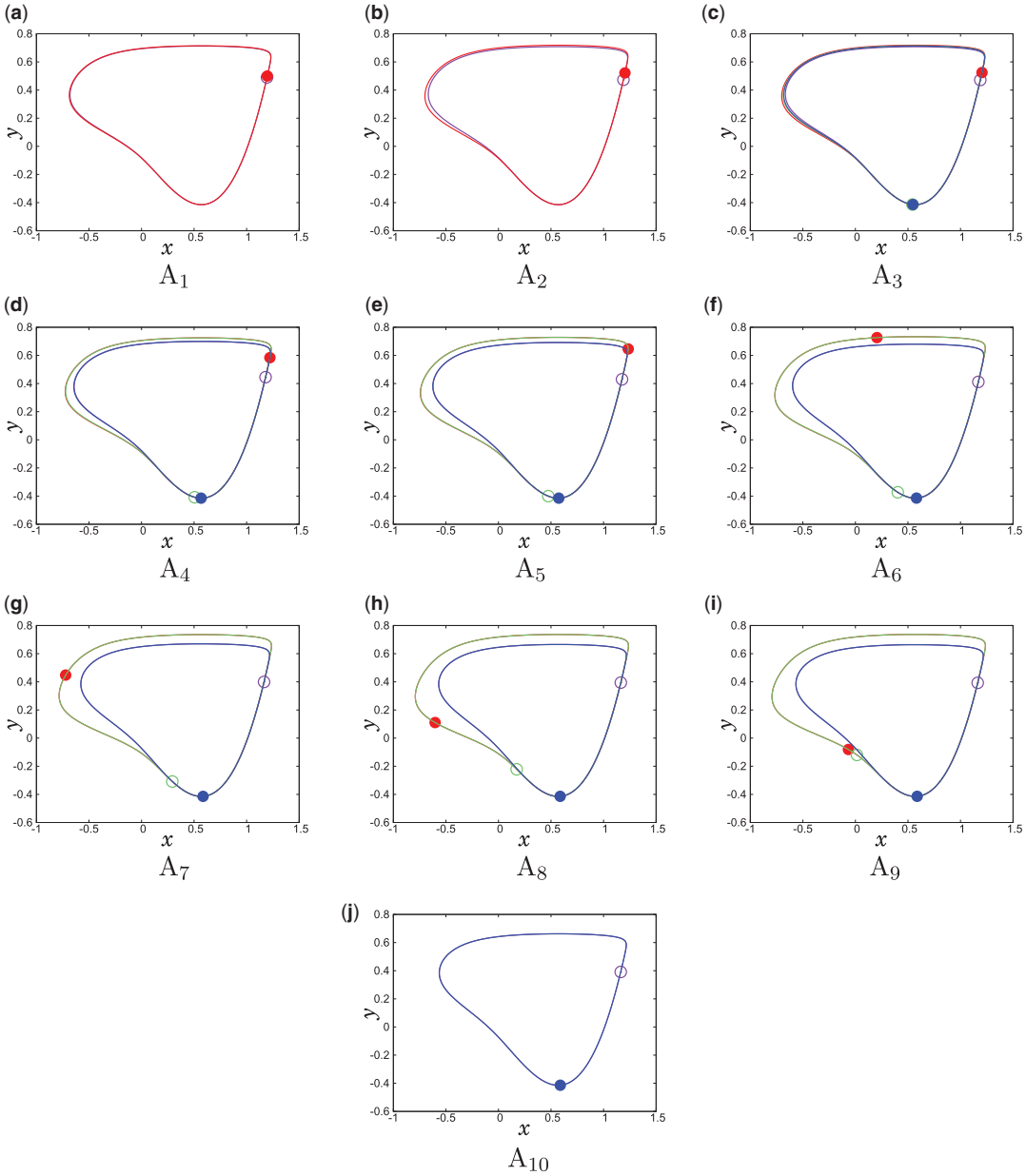

Fig. 9. Four canard solutions: stable canard 1 (red), stable canard 2 (blue), saddle canard 1 (purple), and saddle canard 2 (light green) generated in the fundamental harmonic entrainment region for parameters A_1–A_{10} in Fig. 7. In (a) and (b), only stable canard 1 and saddle canard 1 are shown owing to the bifurcation structure shown in Fig. 7 (lower). Similarly, in (j) only stable canard 2 and saddle canard 1 are shown. Poincaré mapped points are shown on each curve using four kinds of indicators: ● for stable canard 1; ○ for saddle canard 1; ● for stable canard 2; and ○ for saddle canard 2.

where y and y' are the y-components of two of the four canard solutions in Eq. (2), $\overline{y}$ ($\overline{y}'$) is the mean value of y (y'), and $y_i = y(\frac{2\pi i}{2^{20}\omega})$. To calculate the coefficients of resemblance, phase θ is selected such that

$$y(\theta) = 0 \text{ and } \dot{y}(\theta) > 0 \tag{10}$$

is satisfied. Figure 10(a) shows a graph of the correlation coefficients that are obtained along L_1($B = 5 \times 10^{-5}$) and Fig. 10(b) shows a magnified view of Fig. 10(a). In these figures, Q_1, Q_2, and Q_3 are the

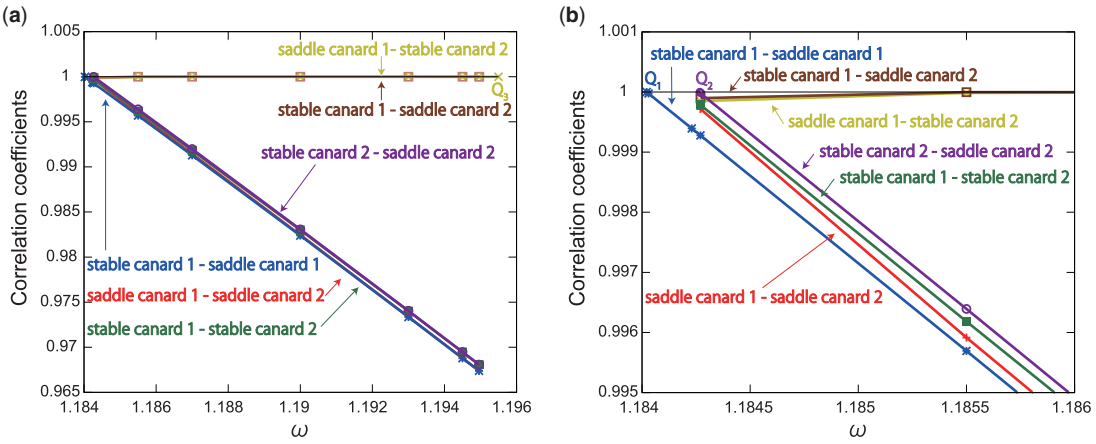

Fig. 10. (a) Graphical representation of the correlation coefficients obtained along L_1 ($B = 5 \times 10^{-5}$) in the fundamental harmonic entrainment region and (b) magnified view of (a).

Table 1. Correlation coefficients for $\varepsilon = 0.1$, $\omega = 1.1855$, and $B = 5.0 \times 10^{-5}$. This choice of parameters corresponds to A_4 in Fig. 7.

	stable canard 1	saddle canard 1	stable canard 2	saddle canard 2
stable canard 1	–	0.995 499 728 345 303	0.995 723 849 285 720	0.999 994 807 767 971
saddle canard 1	–	–	0.999 996 929 396 777	0.995 793 721 722 061
stable canard 2	–	–	–	0.996 010 193 155 091
saddle canard 2	–	–	–	–

saddle-node bifurcation points shown in Fig. 7. At these points, the correlation coefficients between stable canard 1 and saddle canard 1, stable canard 2 and saddle canard 2, and saddle canard 1 and stable canard 2 are 1, because each stable canard coincides with the corresponding saddle canard. As seen in these figures, the correlation coefficients between stable canard 1 and saddle canard 2 and saddle canard 1 and stable canard 2 are close to 1; however, the given parameter value ω is very close to Q_1 and Q_2, which are saddle-node bifurcation points that generate dissimilar canards. In contrast, the correlation coefficients between stable canard 1 and saddle canard 1 and stable canard 2 and the saddle canard 2 decrease proportionally as the bifurcation parameter ω varies from the saddle-node bifurcation points Q_1 and Q_2. Table 1 shows the calculated correlation coefficients for A_4 in Fig. 7, which is located at a slight distance of 0.001 from the saddle-node bifurcation points Q_1 and Q_2. These results indicate that the close respective correlations of stable canards 1 and 2 and saddle canards 2 and 1 are maintained over a wide range of parameters.

If we trace the fixed-point manifold from right to left in Fig. 7, an attractor and saddle solution with a similar shape but with a nontrivial time shift are born at Q_4, whereas a second similar saddle-node bifurcation occurs at Q_3, i.e., Q_3 and Q_4 are saddle-node bifurcation points that generate similar canards.

4. Analysis of two pairs of stable and unstable canards in the 1/2-subharmonic entrainment region

We next investigate the bifurcation structure of the 1/2-subharmonic entrainment region. Because the period of the objective solution is twice that of the fundamental harmonic solution ($4\pi/\omega$) in this subharmonic entrainment region, there exist fixed points on T_λ^2 (twice the composite of T_λ).

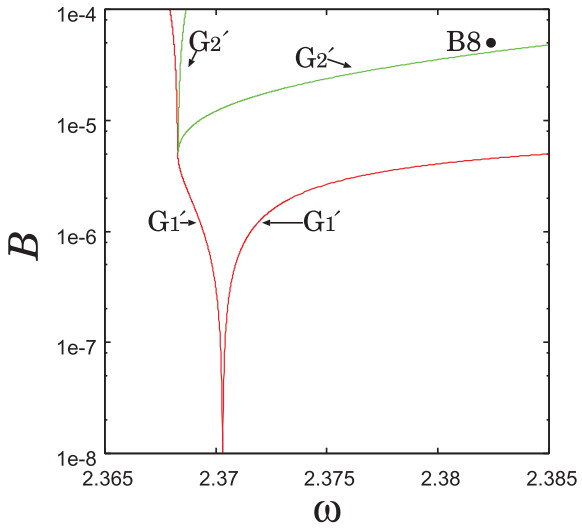

Fig. 11. Bifurcation diagram of the 1/2-subharmonic entrainment region for $\varepsilon = 0.1$ and $B_0 = 0.569\,44$. G_1' and G_2' denote the first and second saddle-node bifurcation sets. The coordinates of B8 are given in Fig. 12.

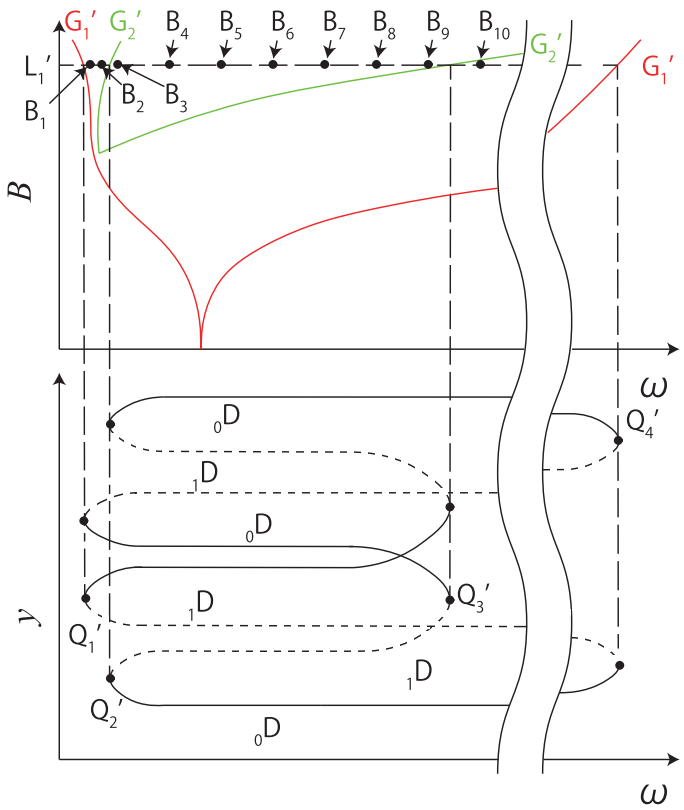

Fig. 12. Schematic bifurcation diagram of the 1/2-subharmonic entrainment region (upper) and the structure of the corresponding periodic-point manifold of T_λ along L_1 (lower). The coordinates (ω,B) of the parameter points B_1–B_{10} are as follows: B_1: $(2.3682, 5 \times 10^{-5})$; B_2: $(2.3684, 5 \times 10^{-5})$; B_3: $(2.3685, 5 \times 10^{-5})$; B_4: $(2.3687, 5 \times 10^{-5})$; B_5: $(2.3689, 5 \times 10^{-5})$; B_6: $(2.37, 5 \times 10^{-5})$; B_7: $(2.375, 5 \times 10^{-5})$; B_8: $(2.3825, 5 \times 10^{-5})$; B_9: $(2.3857, 5 \times 10^{-5})$; B_{10}: $(2.387, 5 \times 10^{-5})$.

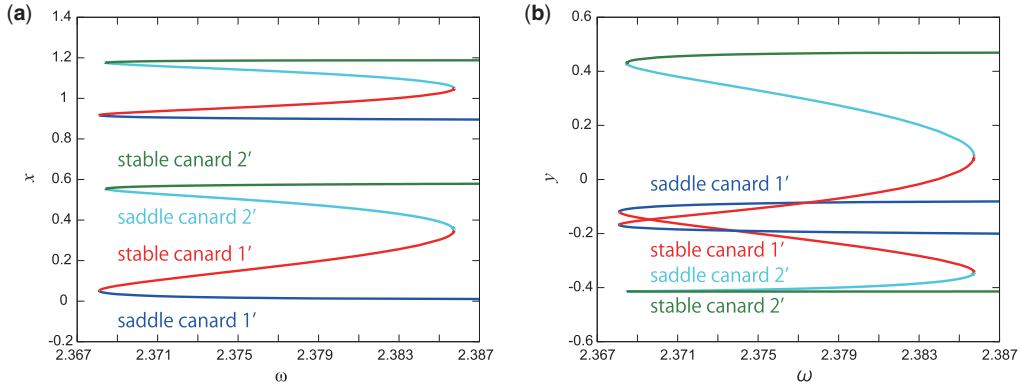

Fig. 13. Periodic-point manifold obtained numerically: (a) projected onto the ω–x plane and (b) projected onto the ω–y plane.

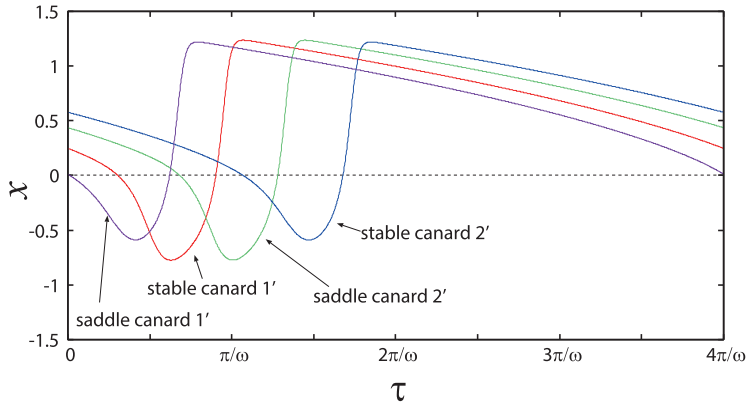

Fig. 14. Time series of the four canard solutions for $\varepsilon = 0.1, \omega = 2.3825, B = 5 \times 10^{-5}$, and $B_0 = 0.569\,44$. This parameter set corresponds to B_8 in Fig. 12.

Figure 11 shows a bifurcation diagram that is obtained by tracing the fixed point of T_λ^2 with the shooting algorithm developed in Ref. [11]. Figure 12 shows an associated schematic illustration of the bifurcation diagram of the 1/2-subharmonic entrainment region. A bifurcation structure similar to that of the fundamental harmonic entrainment region is observed in this entrainment region, i.e., two entrainment regions (one between the two G_1' and the other between the two G_2') exist, and two pairs of stable and saddle canards are present inside the second entrainment region between the two G_2'. Figure 13 shows periodic-point manifolds of T_λ obtained numerically.

In a similar manner, we call the stable and saddle canards arising from the first saddle-node bifurcation denoted by Q_1' stable canard 1′ and saddle canard 1′, respectively. Similarly, we call the stable and saddle canards arising from the second saddle-node bifurcation denoted by Q_2' stable canard 2′ and saddle canard 2′. Figure 14 shows the time series of the four canards. The associated closed orbits projected onto the x–y plane are shown in Figs. 15(a)–(j), where the red solid and purple open circles denote the fixed points associated with stable canard 1′ and saddle canard 1′ on the Poincaré map, respectively. Similarly, the blue solid and green open circles denote, respectively, the fixed points associated with stable canard 2′ and saddle canard 2′ on the Poincaré map. Similar to the case of the fundamental harmonic entrainment region, the red circle (stable canard 1′) moves as ω increases, while the purple circle (saddle canard 1′) does not move significantly when ω increases.

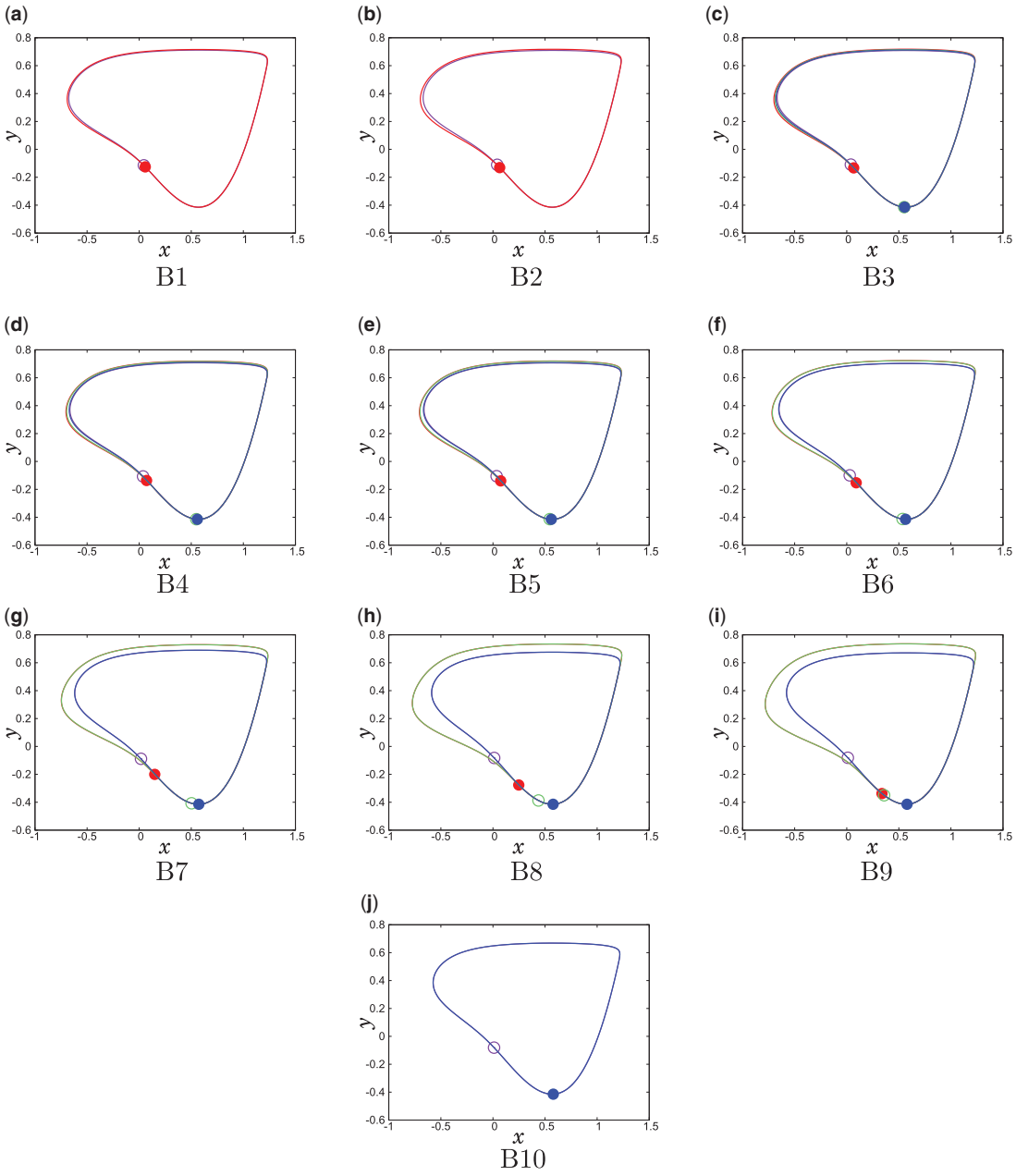

Fig. 15. Four canard solutions: stable canard 1′ (red), stable canard 2′ (blue), saddle canard 1′ (purple), saddle canard 2′ (light green) generated in the 1/2-subharmonic entrainment region for B1–B10 in Fig. 12. In (a) and (b), only stable canard 1′ and saddle canard 1′ are shown owing to the bifurcation structure shown in Fig. 12 (lower). In addition, (j) shows only stable canard 2′ and saddle canard 1′. Poincaré mapped points are shown on each curve as four types of points: ●, for stable canard 1′; ○, for saddle canard 1′; ●, for stable canard 2′; and ○, for saddle canard 2′.

In contrast, the light green open circle (saddle canard 2′) moves and the blue solid circle remains in place when ω increases.

The correlation coefficients are calculated in a manner similar to the previous case by replacing $y_i = y(\frac{4\pi i}{2^{20}\omega})$ in Eq. (9), as these are the solutions for the period $4\pi/\omega$, and their graphs are shown in Fig. 16

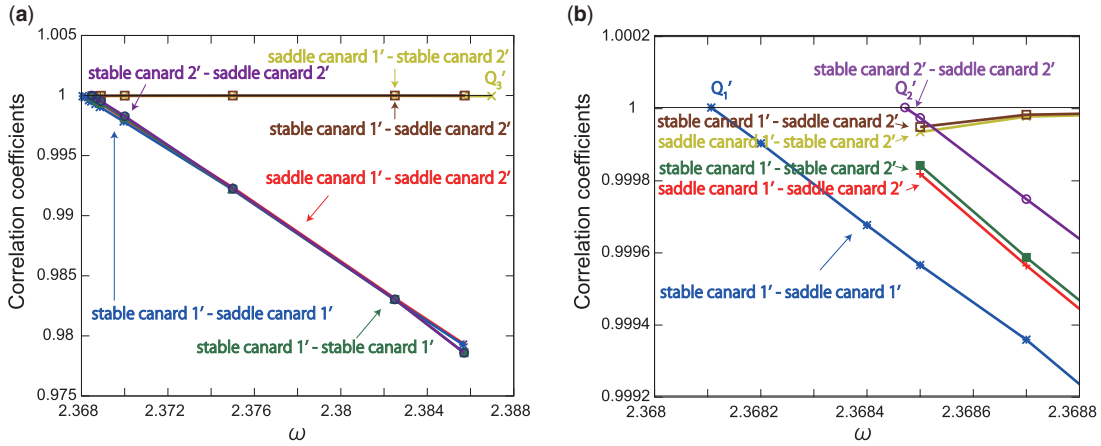

Fig. 16. (a) Graphical representation of the correlation coefficients obtained along L_1' ($B = 5 \times 10^{-5}$) in the 1/2-subharmonic entrainment region and (b) magnified view of (a).

5. Discussion

Finally, we discuss the mechanism underlying the above-described formation of two pairs of similarly shaped stable and saddle canards. We hypothesize that the saddle-node bifurcations denoted by Q_3 and Q_4 occur approximately with the following properties at the bifurcation points:

$$\begin{pmatrix} \dot{x} \\ \dot{y} \end{pmatrix} \approx DT_\lambda(x_Q, y_Q) \begin{pmatrix} \dot{x} \\ \dot{y} \end{pmatrix}, \tag{11}$$

where $DT_\lambda(x_Q, y_Q)$ is a Jacobian matrix of T_λ on $(x_Q, y_Q)^\top$ at the saddle-node bifurcation point. If Eq. (11) approximately holds, the stable and saddle canards arising from the saddle-node bifurcation are nearly invariant for a slight local shift of time.

Table 2 shows data obtained at the four saddle-node bifurcation points. (x_Q, y_Q) indicates the coordinates of the fixed point of T_λ at the saddle-node bifurcation points. (V_x, V_y) represents the eigenvector of DT_λ at (x_Q, y_Q), and p and q represent $\dot{y}/\dot{x}$ and Vy/Vx, respectively. As expected, p is close to q, and $|p-q|/q$ assumes very small values at the saddle-node bifurcation points Q_3 and Q_4. However, $|p-q|/q$ is also small at the saddle-node bifurcation points Q_1 and Q_2. Thus, the resemblance of the stable and saddle canards generated at the saddle-node bifurcation points Q_3 and

Table 2. Four saddle-node bifurcation points of the fundamental harmonic entrainment region and the ratio of $\frac{|p-q|}{q}$, where $p = \frac{\dot{y}}{\dot{x}}$ and $q = \frac{Vy}{Vx}$ ($B_0 = 0.569\,44$).

	ω B	x_Q y_Q	p q	relative error $\lvert p-q\rvert/q$
Q_1	1.184 021 390 $4.999\,834\,920\,781\,219\times10^{-5}$	1.195 685 799 757 652 0.494 777 460 199 819	3.301 883 711 085 376 3.301 471 605 301 792	0.000 124 824 875 950
Q_2	1.184 262 950 $5.000\,288\,167\,891\,380\times10^{-5}$	0.545 121 211 177 124 −0.413 541 347 956 114	−0.079 891 341 437 406 −0.079 978 141 665 362	0.001 086 478 539 407
Q_3	1.194 967 000 $4.999\,665\,534\,199\,296\times10^{-5}$	−0.022 760 396 644 403 −0.100 871 820 029 808	−0.479 047 367 749 357 −0.478 792 815 356 100	0.000 531 654 578 332
Q_4	1.199 500 000 $5.244\,845\,797\,130\,837\times10^{-6}$	0.903 593 931 788 747 −0.188 631 267 550 821	1.465 233 285 927 298 1.465 235 041 979 927	0.000 001 198 478 454

Q_4 can be locally explained to some extent. However, we cannot not distinguish Q_1 and Q_2, which generate dissimilar canards, from Q_3 and Q_4, which generate similar canards.

6. Conclusion

We investigated the resemblances of two pairs of stable and saddle canards in a van der Pol oscillator with extremely weak periodic perturbation. We found that there are two pairs of stable and saddle canards for parameter values in the region surrounded by the second saddle-node bifurcation curves. More explicitly, we clarified that stable canard 1 resembles saddle canard 2 and stable canard 2 resembles saddle canard 1 quite well, although their phases are significantly different, whereas stable canard 1 (stable canard 2) does not resemble saddle canard 1 (saddle canard 2) as closely. In this case, stable canard 1 and saddle canard 1 originated from the first saddle-node bifurcation, while stable canard 2 and saddle canard 2 originated from the second saddle-node bifurcation. We confirmed this resemblance both for the fundamental harmonic entrainment region and the 1/2-subharmonic entrainment region. We investigated the local bifurcation structure at the saddle-node bifurcations, and demonstrated the mechanism causing the resemblance of the two pairs of canards.

Acknowledgements

This work was supported by JSPS KAKENHI Grant Numbers 16K06430 and 16H02876.

References

[1] M. Diener, Math. Intel. **6**, 38 (1984).
[2] A. K. Zvonkin and M. A. Shubin, Russ. Math. Surv. **39**, 69 (1984).
[3] M. Itoh and R. Tomiyasu, Trans. IEICE **E73**, 848 (1990).
[4] M. Broens and K. Bar-Eli, J. Phys. Chem. **95**, 8706 (1991).
[5] V. I. Arnol'd, *Dynamical Systems V* (Berlin, Springer, 1994), Encyclopedia of Mathematical Sciences Vol. 5.
[6] G. Zhao, Z. Hou, and H. Xin, J. Phys. Chem. **109**, 8515 (2005).
[7] M. Brøns, J. Chem. Phys. **134**, 144105 (2011).
[8] J.-M. Ginoux and J. Llibre, J. Phys. A **44**, 465203 (2011).
[9] M. Sekikawa, N. Inaba, T. Yoshinaga, and H. Kawakami, Electron. Comm. Jpn. Pt. III **88**, 51 (2005).
[10] M. Sekikawa, N. Inaba, and K. Aihara, Phys. Lett. A **363**, 404 (2007).
[11] H. Kawakami, IEEE Trans. Circ. Syst. **CAS-31**, 248 (1984).